



HAL
open science

Sub-20 kHz low frequency noise near ultraviolet butt-coupled fiber-Bragg grating external cavity laser diode

R Kervazo, A Congar, G Perin, L Lablonde, R Butté, N Grandjean, L Bodiou,
J Charrier, S Trebaol

► **To cite this version:**

R Kervazo, A Congar, G Perin, L Lablonde, R Butté, et al.. Sub-20 kHz low frequency noise near ultraviolet butt-coupled fiber-Bragg grating external cavity laser diode. Applied Physics Letters, 2024, 125, pp.161102. 10.1063/5.0235240 . hal-04586504v2

HAL Id: hal-04586504

<https://hal.science/hal-04586504v2>

Submitted on 17 Oct 2024

HAL is a multi-disciplinary open access archive for the deposit and dissemination of scientific research documents, whether they are published or not. The documents may come from teaching and research institutions in France or abroad, or from public or private research centers.

L'archive ouverte pluridisciplinaire **HAL**, est destinée au dépôt et à la diffusion de documents scientifiques de niveau recherche, publiés ou non, émanant des établissements d'enseignement et de recherche français ou étrangers, des laboratoires publics ou privés.

Sub-20 kHz low frequency noise near ultraviolet butt-coupled fiber-Bragg grating external cavity laser diode

R. Kervazo¹, G. Perin¹, A. Congar², L. Lablonde³, R. Butté⁴, N. Grandjean⁴, L. Bodiou¹, J. Charrier¹, S. Trebaol^{1,a)}

¹ Univ Rennes, CNRS, Institut FOTON - UMR 6082, F-22305 Lannion, France

² Oxxius, 4 rue Louis de Broglie, 22300 Lannion, France

³ Exail, rue Paul Sabatier, Lannion, France

⁴ Institute of Physics, École Polytechnique Fédérale de Lausanne (EPFL), CH-1015 Lausanne, Switzerland

a) Author to whom correspondence should be addressed: stephane.trebaol@univ-rennes.fr

We present a butt-coupled InGaN fiber Bragg grating (FBG) semiconductor laser diode operating below 400 nm in the single-mode emission regime. This compact coherent laser source exhibits an intrinsic linewidth of 14 kHz in the near-UV range and a side-mode suppression ratio reaching up to 40 dB accompanied by almost 2 mW output power. Furthermore, the properties of the FBG, including its central wavelength, bandwidth, and reflectivity, can be readily customized to fulfill specific requirements. As a result, the small footprint design of this laser is compatible with integration into a standard butterfly package to ease the lab-to-market technology transfer. The combination of low frequency noise and fibered output signal positions these FBG laser systems as strong candidates for hybridization with integrated photonic platforms tailored for quantum information processing and metrology.

Nowadays, laser diodes (LDs) are essential elements for the development of compact photonic devices. They offer the opportunity of combining good performances in terms of linewidth, optical power and frequency noise (FN)[1–3]. The needs in the field of optical telecommunications have enabled the development of compact LDs mainly in the telecom C-band. The implementation of such compact LDs with low-FN at visible wavelengths is a technological challenge recently addressed by several research groups[4–8]. The objective is to provide LDs capable of meeting several application requirements in the fields of classical and quantum sensors and the metrology of optical frequencies for the production of compact optical atomic clocks[9–11]. Indeed, such clocks require the use of narrow-spectrum and low-FN lasers at visible and near-ultraviolet wavelengths for cooling, capturing and manipulating atoms or ions[10,12–14]. Commercial laser devices offering the necessary performances are usually based on an external cavity involving a diffraction grating that does not provide the desired compactness and mechanical robustness for applications outside laboratories. However, recent demonstrations based on compact external cavities, such as integrated optical resonators[4,5] offer interesting perspectives. Despite meeting the compactness requirement, these approaches suffer from reduced figures of merit both in terms of output power (in the μ W range) and linewidth (in the MHz range). Moreover, the performance of state-of-the-art optical clocks is still limited by the FN floor of the lasers used[15].

Indeed, efforts are needed to lower this noise floor by increasing the finesse of the external cavity, which can be obtained by reducing the propagation losses and by increasing the reflectivity of the output mirror. Fiber Bragg gratings[16] (FBGs) are suitable devices for deporting the external cavity in the collection fiber, combining low propagation losses and a wavelength-selective mirror whose reflectivity and bandwidth can be widely adjusted to find the right optical power/finesse trade-off. Moreover, the Bragg center wavelength can be finely adjusted with a sub-0.1 nm accuracy with current fabrication methods[17]. In addition, fiber gratings exhibit a significantly lower sensitivity to temperature fluctuations compared to LD waveguides [18]. This characteristic provides the opportunity to operate without thermal regulation. Initially implemented in the C-band for wavelength-division multiplexing applications[19,20], research works on fiber Bragg grating lasers (FGLs) are now reported at various optical wavelengths[7,21]. Indeed, due to their exceptional wavelength accuracy and stability, fiber gratings can

This is the author's peer reviewed, accepted manuscript. However, the online version of record will be different from this version once it has been copyedited and typeset.

PLEASE CITE THIS ARTICLE AS DOI: 10.1063/1.50235240

serve as frequency references, enabling single-mode laser frequency emissions that precisely align with the requirements of atomic spectroscopy and metrology[9,22].

Despite interesting performances in terms of output power and low FN, previously reported FGL configuration in the near-UV[7] suffered from a lack of integration due to the use of lenses for beam shaping. Indeed, looking for the optimum trade-off between footprint reduction, ease of integration from one side, and optical stability, output power optimization from the other side speaks in favor of a butt-coupled configuration of the FGL. Historically, such an optimized laser configuration has been first implemented in the telecom band, which allowed the lab-to-market technology transfer known as the compact butterfly packaging configuration that became the standard for large scale photonic integration.

In the present work, we propose a more compact solution in the near-ultraviolet spectral range by demonstrating a miniature footprint configuration of a UV LD emitting at 399.6 nm subject to optical feedback from an FBG. The resulting 2 cm external fibered cavity acts as a spectral filter that strongly improves the spectral performance of the initially multimode laser (Fig. 1). Even though shortening the operating wavelength implies an increased complexity in terms of optical alignment, the resulting single-mode laser displays an intrinsic linewidth down to 14 kHz with a mW-fibered-output power together with a 40 dB side-mode suppression ratio (SMSR) thanks to the use of a narrowband FBG. The structure of the LD and the design of the FGL to reach such low FN are first described. Then, the fabrication and characterization steps of the Bragg grating contributing to the external cavity are given. Finally, the spectral performances of the laser, in particular the spectrum and FN measurements, are presented.

The architecture of the single-mode LD is detailed in Fig. 1.

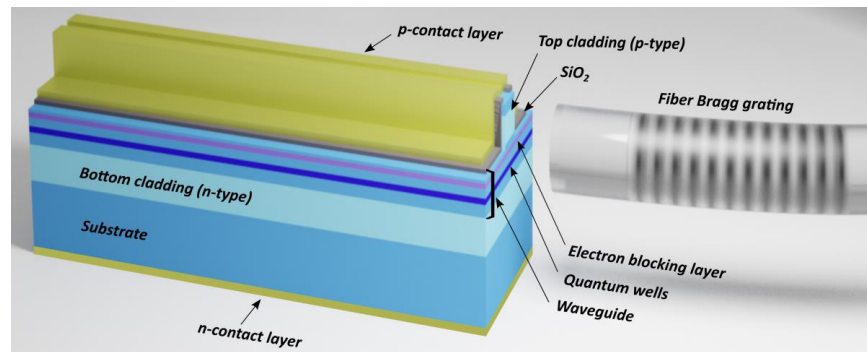


Fig. 1. Schematic of the FBG InGaN LD. Details are given in the Supplementary Material (Sec.1).

The LD stacking was epitaxially grown using the metalorganic vapor phase epitaxy method on a low threading dislocation density ($\sim 10^6 \text{ cm}^{-2}$) *c*-plane free-standing GaN substrate following the same procedure as described in ref.[23]. The optical gain, centered at 400 nm, is provided by two 4.5-nm-wide InGaN quantum wells separated by 12-nm-undoped $\text{In}_{0.05}\text{Ga}_{0.95}\text{N}$ barriers, while a *p*-AlGaN electron-blocking layer is present on the *p*-type side of the junction to avoid any electron overflow. The bottom and top claddings are 1 μm and 500 nm thick, respectively. The epitaxial structure of the diode is shown in the Supplementary Material (Sec. 1). The laser consists of an 800- μm -long ridge structure, which corresponds to a measured Fabry-Perot cavity free spectral range (FSR) of 26 pm. The ridge width is limited to 2.5 μm to ensure single-mode transverse operation. A five-layer dielectric distributed Bragg reflector ($\text{SiO}_2/\text{Ta}_2\text{O}_5$) with a reflectivity R_1 of $\sim 95\%$ was deposited on the back mirror facet to maximize the emission directivity. On the opposite output facet, a single SiO_2 layer drops the reflection R_2 down to $\sim 9\%$ to improve the sensitivity to optical feedback from the FBG and consequently ease the single-mode operation of the laser. Those deposited dielectric layers play a crucial role to prevent LD facet degradation, which is a well-known drawback to maintain long-term laser high performances [24]. The LD temperature fluctuations are reduced to less

This is the author's peer reviewed, accepted manuscript. However, the online version of record will be different from this version once it has been copyedited and typeset.

PLEASE CITE THIS ARTICLE AS DOI: 10.1063/1.50235240

than 0.01 °C using a Peltier controller. This temperature control allows the gain curve to be spectrally tuned by 0.07 nm/K on par with the gain frequency drift values reported in the literature for GaN LDs[25].

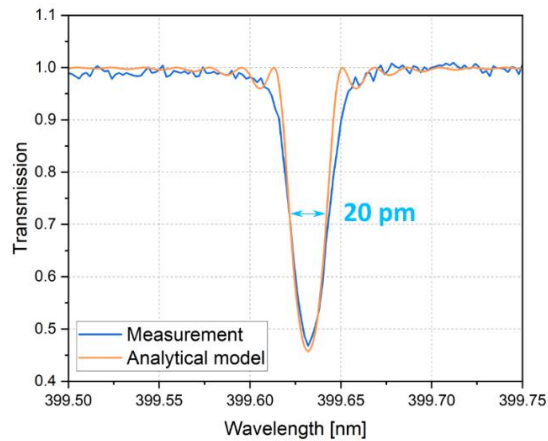


Fig. 2. Fiber Bragg grating transmission measurement (blue curve) and corresponding simulated spectrum (orange curve). The simulation parameters are the following ones: FBG length = 3 mm, index modulation $\Delta n = 0.40 \times 10^{-4}$. More details are given in the Supplementary Material (Sec. 2).

An FBG is associated with the LD to form an external cavity. Thus, to obtain stable single-mode operation and spectral narrowing of the LD under optical feedback, only one longitudinal mode of the LD has to be selected by a full-width-at-half maximum (FWHM) of the Bragg grating reflectivity narrower than the FSR of the multimode LD. The FBG has been designed accordingly.

This mirror is fabricated by exploiting the photosensitivity of a short-wavelength commercially available germanosilicate single-mode fiber. The fiber is transversally exposed to a fringe pattern at a wavelength $\lambda_{uv} = 213$ nm using a 150-mW high-repetition rate nanosecond quintupled Nd:YVO₄ laser[26]. To address the issues for high-quality FBG over Bragg wavelengths ranging from 375 to 410 nm and to achieve Bragg wavelength flexibility, a scanning Talbot interferometer was used[27]. In a near future, femtosecond laser-written FBGs at short wavelengths could be investigated[28,29].

The transmission spectrum of the 3-mm FBG (Fig. 2, blue curve) displays a reflectivity R_3 of 53.5 % and a FWHM evaluated to 20 pm, close to the optical spectrum analyzer (OSA) spectral resolution (10 pm). An analytical model based on coupled mode theory [16] is used to confirm the adequacy of the design with the measured transmission, as shown in Fig. 2 (orange curve). Further details on the simulation procedure are provided in the Supplementary Material (Sec. 2).

This is the author's peer reviewed, accepted manuscript. However, the online version of record will be different from this version once it has been copyedited and typeset.

PLEASE CITE THIS ARTICLE AS DOI: 10.1063/1.50235240

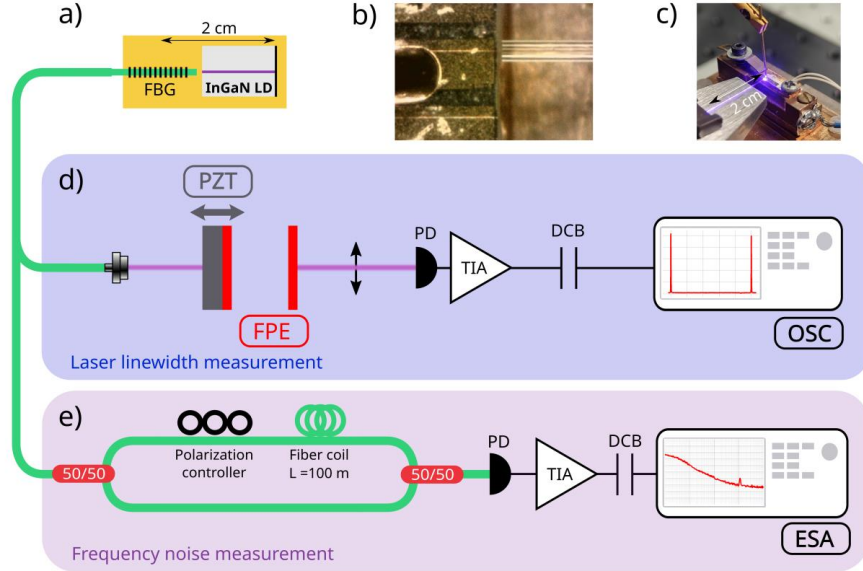


Fig. 3. UV FGL synopsis and characterization benches. a) UV FGL structure. b) Top view picture of the InGaN Fabry-Perot LD butt-coupled to the FBG. c) UV FGL setup with an integrated diode and a cavity length of 2 cm. d) Experimental setup for linewidth measurement based on a Fabry-Perot etalon (FPE). One of the mirrors is linearly translated, thanks to a piezo actuator (PZT), to scan the laser line. e) FN measurements are performed using a correlated delayed self-homodyne measurement setup composed of an imbalanced fiber-based Mach-Zehnder interferometer that plays the role of FN discriminator. The electrical signals generated by photodiodes (PD) are directed to both an oscilloscope (OSC) and an electrical spectrum analyzer (ESA) via transimpedance amplifiers (TIA) and DC-blocks (DCB). For the measurement of DC photocurrents, a multimeter (A) is used. To overcome parasitic feedback in the laser, only angle-polished connectors have been used in the experimental setup.

The external FBG reflector is butt-coupled to the LD as shown in Fig. 3a). The length of the external cavity is less than 2 cm long and the residual airgap d between the cleaved fiber and the LD mirror output is evaluated to be less than $10 \mu\text{m}$. The total footprint of the device corresponds to an area smaller than $0.5 \times 2 \text{ cm}^2$ which is compatible with a commercial butterfly packaging. The optical feedback at the Bragg wavelength of the narrowband FBG aims to select the nearest longitudinal mode of the Fabry-Perot type semiconductor laser. This can be obtained since the FBG linewidth (20 pm) is narrower than the LD FSR (26 pm). Such butt-coupled approach avoids the use of bulky lenses as in extended external cavity approaches hence improving the robustness to mechanical vibrations and thus the spectral performances.

To get an idea of the importance of the coupling efficiency on the laser UV FGL performances, we can approximate the efficiency of the optical feedback by considering the effective reflectivity of the fiber Bragg grating, which takes into account the coupling between the fiber and the LD as[30]:

$$R_{2,eff} = \eta^2 \times R_3, \quad (1)$$

where η is the coupling coefficient between the fiber and the diode and R_3 is the FBG reflectivity at the Bragg wavelength discussed earlier. Considering the approximation of Gaussian beams, the coupling efficiency as a function of the distance between the two components is given by[31]:

$$\eta(d) = \frac{4 \times \omega_{LD,x} \times \omega_{LD,y} \times \omega_{fiber}^2}{\sqrt{(\omega_{LD,x}^2 + \omega_{fiber,x}^2)^2 + \left(\frac{2d}{k}\right)^2} \sqrt{(\omega_{LD,y}^2 + \omega_{fiber,y}^2)^2 + \left(\frac{2d}{k}\right)^2}}, \quad (2)$$

where $\omega_{LD,i}$ is the waist of the laser diode in the i -direction, ω_{fiber} is the waist of the fiber, k is the wave vector expressed as $\frac{2\pi}{\lambda}$ and d is the residual airgap between the cleaved fiber and the LD mirror output. In order to get an estimation of the maximal theoretical coupling coefficient that can be reached with this configuration, we performed beam waist measurements of the LD and the fiber (see sections 3 and 4 in the supplementary materials) and obtained $\omega_{LD,x} = 0.74 \mu\text{m}$, $\omega_{LD,y} = 0.30 \mu\text{m}$ and $\omega_{fiber} = 1.58 \mu\text{m}$. By injecting those parameters in Eq. (2), the coupling coefficient of our system can be plotted as a function of d , the distance separating the LD and the FBG input facet (Fig. 4).

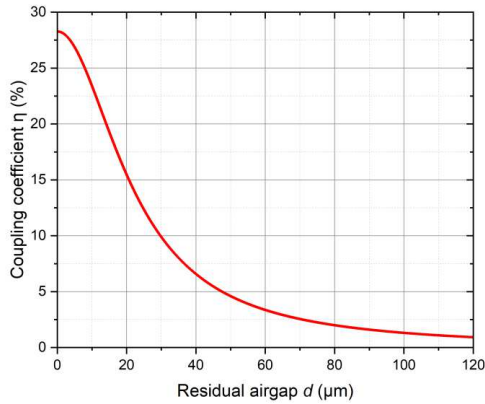


Fig. 4. Coupling coefficient η of the UV FGL laser as a function of the residual airgap between the cleaved fiber and the LD mirror output

The residual airgap, d , is tuned to optimize the strength of the feedback taking into account the FP effect of the airgap cavity (see supplementary materials, Sec. 5). According to this, the estimated coupling efficiency at this distance is $\eta \sim 23\%$.

With a coupling coefficient of 23% and a FBG reflectivity of 55%, we obtain an $R_{2,\text{eff}}$ value equal to 2.9%, which is lower than the output facet reflectivity of the LD ($R_2 = 9\%$). In our previous configuration[7], the effective reflectivity was higher than the output facet reflectivity. According to Ref.[32], removing the lenses therefore results in a miniaturization of the system but also modifies the feedback regime. The previous configuration was in the strong feedback regime (corresponding to regime V as described in Ref.[32]) while the FGL presented in the present work lies in the perturbative regime III. Both regimes lead to linewidth narrowing of the LD from the filtered optical feedback of the external cavity. Let us note that further investigations on the impact of the feedback regime on the frequency intensity noises [33] would likely give some useful insights into the improvement of the design of miniature butt-coupled external cavity diode lasers.

The optical spectrum of the LD was first characterized without Bragg grating (gray curve in Fig. 5a). Without feedback, the optical spectrum of the LD reveals multimode operation with a maximum SMSR on the order of 20 dB. By carefully aligning the FBG in front of the Fabry-Perot LD output, the optical spectrum collapses in stable single-mode operation. Thus, in its FGL configuration, the laser spectrum bandwidth is drastically reduced and exhibits single-mode lasing operation at the Bragg wavelength with a 40 dB SMSR for a pump current of 124 mA. The FGL output power can reach up to 1.8 mW at 399.6 nm corresponding approximately to 3.9 mW at the InGaN LD output facet (see Supplementary Material Sec. 6).

This is the author's peer reviewed, accepted manuscript. However, the online version of record will be different from this version once it has been copyedited and typeset.

PLEASE CITE THIS ARTICLE AS DOI: 10.1063/1.50235240

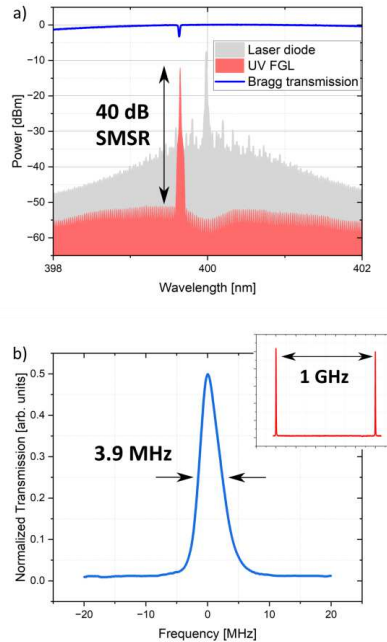


Fig. 5. Spectral characterization of the UV FGL. a) Optical spectra of the LD (gray curve) and the UV FGL (red curve) for a pump current of 124 mA. The blue curve corresponds to the fiber Bragg transmission centered at 399.6 nm. b) Optical spectrum of the UV FGL obtained with an FPE (3.9 MHz spectral resolution and 1 GHz FSR). Inset) Optical spectrum measurement through the FPE confirming that the UV FGL behaves in the single longitudinal-mode regime.

Since the OSA resolution is not sufficient to prove single-mode operation, the spectral performances of the FGL are then studied using the characterization bench displayed in Fig. 3d). The high-resolution measurements of the optical spectrum were carried out with a Fabry-Perot etalon (FPE). The result is presented in the inset of Fig. 5b). Two peaks separated by 1 GHz, corresponding to the FSR of the FPE, confirmed that the FGL oscillates on a single mode of the external cavity. However, as the width of the measured peak (3.9 MHz) corresponds to the spectral resolution of the FPE, this feature cannot be used to evaluate correctly the optical linewidth.

A self-homodyne[34] characterization bench based on a Mach-Zehnder [35] interferometer was built (Fig. 3e)) to determine the actual FN of the laser. The description of the bench is given in supplementary material (Sec. 7). This setup enables laser FN analysis over a frequency bandwidth ranging from 100 Hz to 2 MHz. The noise floor reaches up to 1000 Hz²/Hz at low frequencies and drop down to few Hz²/Hz above 100 kHz. Fig. 6a) shows the result of the measurements. The red curve represents the characterization of the FN of the UV FGL laser at 399.6 nm. For the sake of comparison, the FN of a commercial external cavity diode laser (ECDL, model Toptica DL Pro) used for Sr-ion cooling and Rb Rydberg excitation at 420.0 nm is also shown (blue curve).

Usually, the FN of a laser is characterized by a white noise of amplitude h_0 at high frequencies, which refers to the intrinsic linewidth of the laser and the noise at low Fourier frequencies whose slope changes in $\frac{1}{f^\alpha}$ with $1 < \alpha < 2$, which corresponds to slow frequency drifts of the intrinsic linewidth[36]. This last contribution is associated with the Gaussian profile which, convolved with the Lorentzian shape intrinsic linewidth, gives the Voigt profile of the laser[37]. It is possible, from measurements of the FN, to estimate the laser linewidth using the Elliott formula [38] (see Supplementary Materials Sec. 8) or by using the beta-line approach [39].

This is the author's peer reviewed, accepted manuscript. However, the online version of record will be different from this version once it has been copyedited and typeset.

PLEASE CITE THIS ARTICLE AS DOI: 10.1063/1.50235240

The FN of the FGL exhibits a plateau for frequency values above 300 kHz corresponding to the white noise associated with the intrinsic linewidth of the laser, which is mainly determined by the noise due to spontaneous emission. A value of $h_0 = 4149 \text{ Hz}^2/\text{Hz}$ gives an estimate of the intrinsic linewidth, through the Elliott formula, of the order of $14 \pm 2 \text{ kHz}$. The intrinsic linewidth is about one order of magnitude smaller than that of the Toptica DL Pro linewidth ($120 \pm 19 \text{ kHz}$). The integration of the FN spectral density and in particular the low-frequency contribution gives access to an estimate of the Voigt profile with a linewidth on the order of $720 \pm 120 \text{ kHz}$ similar to the performances of the Toptica DL Pro. Indeed, both acoustic and mechanical noises perturb the FGL central frequency, contributing to the broadening of the linewidth for longer integration times. Locking the laser to a more stable frequency reference [35] could provide a solution to overcome this technical noise affecting the emission frequency. The relative intensity noise (RIN) characterization of the UV FGL is reported in Fig. 6 b). The RIN level is evaluated to -123 dB/Hz for Fourier frequencies below the oscillation relaxation frequency centered at $\sim 2 \text{ GHz}$.

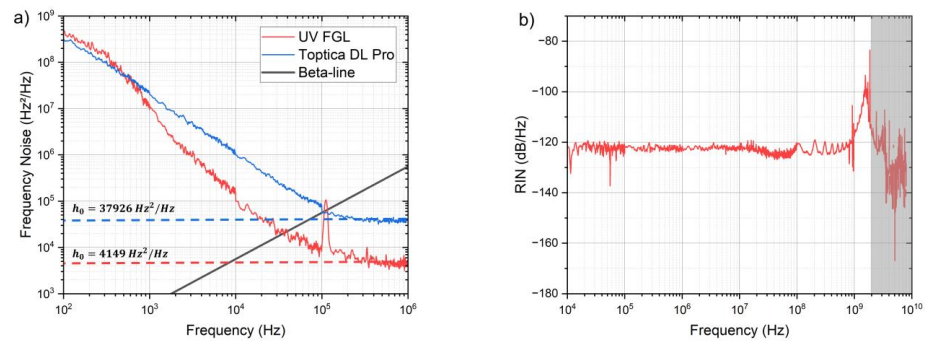


Fig. 6. a) FN measurements of the UV FGL at 399.6 nm (red color) and Toptica DL Pro emitting at 420.0 nm (blue color). The peak seen at $\sim 100 \text{ kHz}$ on the red curve is due to the PD noise. The beta-line can be used to estimate the integrated linewidth [39] b) RIN measurement on the UV FGL in single mode operation. The gray section delimits the detection range limited by the 2 GHz photodiode bandwidth.

A comparison with similar hybrid or integrated ECDL systems is proposed in Table I. This comparison is based on a table-top commercial solution and state-of-the-art integrated ECDL lasers. The Toptica DL Pro is a renowned commercial ECDL proposing a high fibered output power of 45 mW with a narrow-integrated linewidth of 887 kHz at 10 ms of integration time. Nevertheless, its dimensions prevent it from further integration in new commercial devices requiring high level of compactness. Compact ECDL laser solutions based on volume holographic grating (Ondax) exist and offer quite large output power but at the expense of a broader linewidth ($> 100 \text{ MHz}$).

To ensure compatibility with a butterfly package, the dimensions of the reported FGL laser were reduced by removing the lenses used for beam shaping. The presented device enables a significant improvement in terms of intrinsic linewidth surpassing previously reported demonstrations[5,6] based on compact external cavity semiconductor lasers by at least two orders of magnitude. This parameter is of prime importance to improve the locking performance of compact optical atomic clocks[15]. Moreover, the FGL laser output power can reach up to 1.8 mW at 399.6 nm, which is up to 100 times larger than the optical powers reported so far for such compact approaches in the near-UV range, which can be accounted for by the fact that integrated optics approaches in this spectral range still suffer from large optical propagation losses[6] and high laser-to-chip coupling losses[5] that degrade the lasing performances.

This is the author's peer reviewed, accepted manuscript. However, the online version of record will be different from this version once it has been copyedited and typeset.

PLEASE CITE THIS ARTICLE AS DOI: 10.1063/5.0235240

Table I : Comparison of external cavity laser diodes emitting in the 400-420 nm range reported in the literature.

Device / Research team	Year	ECDL Technology	λ (nm)	SMSR (dB)	Fibered output power (mW)	Linewidth		Butterfly package compatibility
						intrinsic	integrated	
Ondax LD [40]		Volume holographic grating	405	40	40 (not fibered)		160 MHz	✓
Toptica DL Pro [41]		Reflective diffraction grating	420	47	45	150 kHz	887 kHz at 10 ms	✗
Congar <i>et al.</i> [7]	2021	Fiber Bragg grating	400	44	1.3	16 kHz	950 kHz at 10 ms	✗
This work	2024	Fiber Bragg grating	400	40	1.8	14 kHz	704 kHz at 10 ms	✓
Corato-Zanarella <i>et al.</i> [5]	2022	Integrated microring	404	21	0.02	< 1.5 MHz (estimated)	3.3 MHz	✓
Franken <i>et al.</i> [6]	2023	Integrated microring	405	43	0.74		< 25 MHz	✓

In summary, by butt-coupling an InGaN semiconductor LD emitting near 400 nm to an FBG, we demonstrated a compact narrow-linewidth semiconductor laser with a Lorentzian linewidth as low as 14 kHz corresponding to a white FN below 5000 Hz²/Hz. This mW-output power laser fulfills the low-FN performances required for atomic spectroscopy and frequency metrology, offering the possibility to develop compact optical atomic clocks [10] and portable quantum sensors [42] based on electronic transitions occurring in the near-UV range [14] as for example, the excitation of the ytterbium Rydberg state at 399 nm for quantum information processing. The compactness, wavelength versatility and ease of access of the fibered output signal represent a promising trade-off between compactness and performances that should favor the hybridization of such an FGL with integrated photonic platforms for quantum information processing[43,44].

Supplementary Material

See the supplementary material for more information including: (1) LD epitaxial structure; (2) FBG design; (3) evaluation of the coupling efficiency between a LD and a fiber; (4) measurement of the mode field diameter; (5) discussion about the impact of the airgap distance over the optical feedback strength; (6) discussion about the output power versus SMSR; (7) description of the FN measurement bench; (8) method to retrieve the optical spectrum from FN measurements.

Data availability

The data that support the findings of this study are available from the corresponding author upon reasonable request.

Author declarations

Conflict of interest

The authors have no conflicts to disclose.

Authors contributions

Ronan Kervazo: Data curation (equal); Conceptualization (equal); Formal analysis (equal); Writing - original draft (equal); Writing - review & editing (equal). **Georges Perin:** Conceptualization (equal); Data curation (equal); Formal analysis (equal); Writing - original draft (equal); Writing - review & editing (equal). **Antoine Congar:** Conceptualization (equal); Formal analysis (equal); Writing - review & editing (equal). **Laurent Lablonde:** Conceptualization (equal); Writing - review & editing (equal). **Raphaël Butté:** Writing - review & editing (equal). **Nicolas Grandjean:** Writing - review & editing (equal). **Loïc Bodiou:** Conceptualization (equal); Formal analysis (equal); Writing - review & editing (equal). **Joel Charrier:** Conceptualization (equal); Formal analysis (equal); Writing - review & editing (equal). **Stéphane Trebaol:** Conceptualization (equal); Supervision (lead); Writing - original draft (equal); Writing - review & editing (equal).

Funding

The present work is supported under projects UV4Life (contract N° 19005486), the European Regional Development Fund (contract N° EU000998), ANR COMBO (contract N° ANR-18-CE24-0003), Région Bretagne and Lannion Trégor Communauté.

References

1. C. Porter, S. Zeng, X. Zhao, and L. Zhu, "Hybrid integrated chip-scale laser systems," *APL Photonics* **8**(8), 080902 (2023).
2. W. Liang, V. S. Ilchenko, D. Eliyahu, A. A. Savchenkov, A. B. Matsko, D. Seidel, and L. Maleki, "Ultralow noise miniature external cavity semiconductor laser," *Nat. Commun.* **6**(1), 7371 (2015).
3. W. Loh, F. J. O'Donnell, J. J. Plant, M. A. Brattain, L. J. Missaggia, and P. W. Juodawlkis, "Packaged, high-power, narrow-linewidth slab-coupled optical waveguide external cavity laser (SCOWECL)," *IEEE Photonics Technol. Lett.* **23**(14), 974–976 (2011).
4. A. Siddharth, T. Wunderer, G. Lihachev, A. S. Voloshin, C. Haller, R. N. Wang, M. Teepe, Z. Yang, J. Liu, J. Riemensberger, N. Grandjean, N. Johnson, and T. J. Kippenberg, "Near ultraviolet photonic integrated lasers based on silicon nitride," *APL Photonics* **7**(4), 046108 (2022).
5. M. Corato-Zanarella, A. Gil-Molina, X. Ji, M. C. Shin, A. Mohanty, and M. Lipson, "Widely tunable and narrow-linewidth chip-scale lasers from near-ultraviolet to near-infrared wavelengths," *Nat. Photon.* **17**(2), 157–164 (2023).
6. C. A. A. Franken, W. A. P. M. Hendriks, L. V. Winkler, M. Dijkstra, A. R. do Nascimento Jr, A. van Rees, M. R. S. Mardani, R. Dekker, J. van Kerkhof, P. J. M. van der Slot, S. M. García-Blanco, and K.-J. Boller, "Hybrid integrated near UV lasers using the deep-UV Al₂O₃ platform," (2023).
7. A. Congar, M. Gay, G. Perin, D. Mammez, J.-C. Simon, P. Besnard, J. Rouvillain, T. Georges, L. Lablonde, T. Robin, and S. Trebaol, "Narrow linewidth near-UV InGaN laser diode based on external cavity fiber Bragg grating," *Opt. Lett.* **46**(5), 1077–1080 (2021).
8. D. J. Blumenthal, "Photonic integration for UV to IR applications," *APL Photonics* **5**(2), 020903 (2020).
9. Z. L. Newman, V. Maurice, T. Drake, J. R. Stone, T. C. Briles, D. T. Spencer, C. Fredrick, Q. Li, D. Westly, B. R. Ilic, B. Shen, M.-G. Suh, K. Y. Yang, C. Johnson, D. M. S. Johnson, L. Hollberg, K. J. Vahala, K. Srinivasan, S. A. Diddams, J. Kitching, S. B. Papp, and M. T. Hummon, "Architecture for the photonic integration of an optical atomic clock," *Optica* **6**(5), 680–685 (2019).
10. V. Maurice, V. Maurice, Z. L. Newman, Z. L. Newman, S. Dickerson, M. Rivers, J. Hsiao, P. Greene, M. Mescher, J. Kitching, M. T. Hummon, and C. Johnson, "Miniaturized optical frequency reference for next-generation portable optical clocks," *Opt. Express* **28**(17), 24708–24720 (2020).

This is the author's peer reviewed, accepted manuscript. However, the online version of record will be different from this version once it has been copyedited and typeset.

PLEASE CITE THIS ARTICLE AS DOI: 10.1063/5.0235240

11. A. Gusching, J. Millo, I. Ryger, R. Vicarini, M. A. Hafiz, N. Passilly, and R. Boudot, "Cs microcell optical reference with frequency stability in the low 10^{-13} range at 1 s," *Opt. Lett.* **48**(6), 1526–1529 (2023).
12. A. A. Savchenkov, J. E. Christensen, D. Hucul, W. C. Campbell, E. R. Hudson, S. Williams, and A. B. Matsko, "Application of a self-injection locked cyan laser for barium ion cooling and spectroscopy," *Sci Rep* **10**(1), 16494 (2020).
13. N. Poli, M. Schioppo, S. Vogt, St. Falke, U. Sterr, Ch. Lisdat, and G. M. Tino, "A transportable strontium optical lattice clock," *Appl. Phys. B* **117**(4), 1107–1116 (2014).
14. K. Enomoto, N. Hizawa, T. Suzuki, K. Kobayashi, and Y. Moriwaki, "Comparison of resonance frequencies of major atomic lines in 398–423 nm," *Appl. Phys. B* **122**(5), 126 (2016).
15. Z. L. Newman, V. Maurice, C. Fredrick, T. Fortier, H. Leopardi, L. Hollberg, S. A. Diddams, J. Kitching, and M. T. Hummon, "High-performance, compact optical standard," *Opt. Lett.* **46**(18), 4702–4705 (2021).
16. R. Kashyap, *Fiber Bragg Gratings*, 2nd ed. (Academic Press, San Diego, 2009).
17. J.-L. Archambault and S. G. Grubb, "Fiber gratings in lasers and amplifiers," *J. Lightwave Technol.* **15**(8), 1378–1390 (1997).
18. S. A. Vasil'ev, O. I. Medvedkov, I. G. Korolev, A. S. Bozhkov, A. S. Kurkov, and E. M. Dianov, "Fibre gratings and their applications," *Quantum Electron.* **35**(12), 1085 (2005).
19. C. R. Giles, "Lightwave applications of fiber Bragg gratings," *J. Lightwave Technol.* **15**(8), 1391–1404 (1997).
20. J. I. Hashimoto, T. Takagi, T. Kato, G. Sasaki, M. Shigehara, K. Murashima, M. Shiozaki, and T. Iwashima, "Fiber-Bragg-grating external cavity semiconductor laser (FGL) module for DWDM transmission," *J. Lightwave Technol.* **21**(9), 2002–2009 (2003).
21. X. Li, J. Shi, L. Wei, K. Ding, Y. Ma, K. Sun, Z. Li, Y. Qu, L. Li, Z. Qiao, G. Liu, L. Zeng, and D. Xu, "Research progress of wide tunable Bragg grating external cavity semiconductor lasers," *Materials* **15**(22), 8256 (2022).
22. C. D. Macrae, K. Bongs, and M. Holynski, "Optical frequency generation using fiber Bragg grating filters for applications in portable quantum sensing," *Opt. Lett.* **46**(6), 1257–1260 (2021).
23. J. Dorsaz, A. Castiglia, G. Cosendey, E. Feltin, M. Rossetti, M. Duellk, C. Velez, J.-F. Carlin, and N. Grandjean, "AlGaIn-free blue III–nitride laser diodes grown on *c*-plane GaN substrates," *Appl. Phys. Express* **3**(9), 092102 (2010).
24. T. Schoedl, U. T. Schwarz, S. Miller, A. Leber, M. Furtsch, A. Lell, and V. Härle, "Facet degradation of (Al,In)GaIn laser diodes," *phys. stat. sol. (a)* **201**(12), 2635–2638 (2004).
25. C. Eichler, S.-S. Schad, F. Scholz, D. Hofstetter, S. Müller, A. Weimar, A. Lell, and V. Harle, "Observation of temperature-independent longitudinal-mode patterns in violet-blue InGaIn-based laser diodes," *IEEE Photonics Technol. Lett.* **17**(9), 1782–1784 (2005).
26. B. Berrang, L. Polz, R. Kuttler, J. Bartschke, and J. Roths, "FBG inscription in non-hydrogenated SMF28 fiber with a ns Q-switched Nd:VO₄ laser at 213 nm," in *Fifth European Workshop on Optical Fibre Sensors* (SPIE, 2013), **8794**, pp. 309–312.
27. M. Becker, J. Bergmann, S. Brückner, M. Franke, E. Lindner, M. W. Rothhardt, and H. Bartelt, "Fiber Bragg grating inscription combining DUV sub-picosecond laser pulses and two-beam interferometry," *Opt. Express* **16**(23), 19169–19178 (2008).
28. K. Zhou, M. Dubov, C. Mou, L. Zhang, V. K. Mezentsev, and I. Bennion, "Line-by-line fiber Bragg grating made by femtosecond laser," *IEEE Photonics Technol. Lett.* **22**(16), 1190–1192 (2010).
29. M. Becker, T. Elsmann, A. Schwuchow, M. Rothhardt, S. Dochow, and H. Bartelt, "Fiber Bragg gratings in the visible spectral range with ultraviolet femtosecond laser inscription," *IEEE Photonics Technol. Lett.* **26**(16), 1653–1656 (2014).
30. K. Petermann, *Laser Diode Modulation and Noise* (Springer Science & Business Media, Berlin, 1991).
31. M. Saruwatari and K. Nawata, "Semiconductor laser to single-mode fiber coupler," *Appl. Opt.* **18**(11), 1847–1856 (1979).
32. R. Tkach and A. Chraplyvy, "Regimes of feedback effects in 1.5- μ m distributed feedback lasers," *J. Lightwave Technol.* **4**(11), 1655–1661 (1986).
33. Y. Hong, S. Bandyopadhyay, S. Sivaprakasam, P. S. Spencer, and K. A. Shore, "Noise characteristics of a single-mode laser diode subject to strong optical feedback," *Journal of Lightwave Technology* **20**(10), 1847–1850 (2002).

This is the author's peer reviewed, accepted manuscript. However, the online version of record will be different from this version once it has been copyedited and typeset.

PLEASE CITE THIS ARTICLE AS DOI: 10.1063/5.0235240

34. O. Llopis, P. H. Merrer, H. Brahim, K. Saleh, and P. Lacroix, "Phase noise measurement of a narrow linewidth CW laser using delay line approaches," *Opt. Lett.* **36**(14), 2713–2715 (2011).
35. G. Perin, D. Mammez, A. Congar, P. Besnard, K. Manamanni, V. Roncin, F. D. Burck, and S. Trebaol, "Compact fiber-ring resonator for blue external cavity diode laser stabilization," *Opt. Express* **29**(23), 37200–37210 (2021).
36. F. Riehle, *Frequency Standards: Basics and Applications* (Wiley-VCH, Weinheim, 2004).
37. G. M. Stéphan, T. T. Tam, S. Blin, P. Besnard, and M. Têtu, "Laser line shape and spectral density of frequency noise," *Phys. Rev. A* **71**(4), 043809 (2005).
38. D. S. Elliott, R. Roy, and S. J. Smith, "Extracavity laser band-shape and bandwidth modification," *Phys. Rev. A* **26**(1), 12–18 (1982).
39. G. Di Domenico, S. Schilt, and P. Thomann, "Simple approach to the relation between laser frequency noise and laser line shape," *Appl. Opt.* **49**(25), 4801 (2010).
40. Ondax, "Ondax laser diode datasheet," <https://www.laserdiodesource.com/laser-diode-product-page/single-frequency-laser-150mW-ondax>.
41. "Toptica DL pro datasheet," <https://www.toptica.com/products/tunable-diode-lasers/ecdl-dfb-lasers/dl-pro>.
42. C. L. Degen, F. Reinhard, and P. Cappellaro, "Quantum sensing," *Rev. Mod. Phys.* **89**(3), 035002 (2017).
43. R. J. Niffenegger, J. Stuart, C. Sorace-Agaskar, D. Kharas, S. Bramhavar, C. D. Bruzewicz, W. Loh, R. T. Maxson, R. McConnell, D. Reens, G. N. West, J. M. Sage, and J. Chiaverini, "Integrated multi-wavelength control of an ion qubit," *Nature* **586**(7830), 538–542 (2020).
44. K. K. Mehta, C. Zhang, M. Malinowski, T.-L. Nguyen, M. Stadler, and J. P. Home, "Integrated optical multi-ion quantum logic," *Nature* **586**(7830), 533–537 (2020).